

Research progress in lead-less or lead-free three-dimensional perovskite absorber materials for solar cells

Huan-yu Zhang¹⁾, Rui Li¹⁾, Wen-wu Liu²⁾, Mei Zhang¹⁾, and Min Guo¹⁾

1) School of Metallurgical and Ecological Engineering, University of Science and Technology Beijing, Beijing 100083, China

2) State Key Laboratory of Advanced Processing and Recycling of Nonferrous Metals, Lanzhou University of Technology, Lanzhou 730050, China

(Received: 24 August 2018; revised: 16 November 2018; accepted: 24 November 2018)

Abstract: The trend toward lead-free or lead-less perovskite solar cells (PSCs) has attracted increasing attention over the past few years because the toxicity of lead (Pb) is one of the substantial restrictions for large-scale applications. Researchers have investigated the viability of substituting Pb with other elements (group 14 elements, group 2 elements, transition-metal elements, and group 13 and 15 elements) in the three-dimensional (3D) perovskites by theoretical calculations and experimental explorations. In this paper, recent research progress in Pb-less and Pb-free PSCs on the perovskite compositions, deposition methods, and device structures are summarized and the main problems that hinder the enhancement of device efficiency and stability are discussed in detail. To date, the fully Sn-based PSCs have shown a power conversion efficiency (PCE) of 8.12% and poor device stability. However, lead-less PSCs have shown higher PCE and a better stability. In addition, the introduction of double-perovskite materials also draws researchers' attention. We believe that the engineering of elemental composition, perovskite deposition methods, and interfacial modification are critical for the future development of Pb-less and Pb-free PSCs.

Keywords: perovskite solar cells; lead-free perovskite materials; lead-less perovskite materials; composition engineering; stability

1. Introduction

The development of dye-sensitized solar cells (DSSCs) has slowed in recent years. The power conversion efficiency (PCE) of these devices is difficult to increase because of dyes' limited light-harvesting ability. In 2009, Miyasaka's group used organic–inorganic hybrid perovskite materials ($\text{CH}_3\text{NH}_3\text{PbI}_3$ and $\text{CH}_3\text{NH}_3\text{PbBr}_3$) as a dye in a DSSC for the first time [1]. Although the perovskite dyes decomposed easily in the liquid electrolyte, the device showed a PCE of 3.8%. Since then, inorganic–organic perovskite materials (e.g., $\text{CH}_3\text{NH}_3\text{PbI}_3$) have been a research hotspot in the photovoltaics field because of their excellent semiconductor properties, which include a narrow bandgap, high absorption coefficient, high carrier mobility, and low exciton binding energy [2–5]. In 2012, the use of solid hole-transporting materials (HTMs) remarkably improved the devices' PCE and stability [6]; these all-solid perovskite-based photovoltaic devices were collectively called perovskite solar cells

(PSCs). To date, PSCs have achieved a certified PCE of 23.3% [7]. Their low fabrication cost and compatibility with solution-processing methods make the commercialization of PSCs viable.

PSCs have three basic structures: mesoscopic, planar, and inverted architectures [8]. The mesoscopic PSCs, which contained metallic oxide nanostructures (e.g., nanoparticles, nanotubes, nanosheets, or nanorods) as electron transporting materials (ETMs), are evolved from DSSCs, and the device structure is often denoted as “Transparent conductive oxide (TCO)/compact ETM/nanostructured ETM/perovskite/HTM/back electrode” (see Fig. 1(a)) [9–11]. The role of these nanostructured ETMs is to enhance light harvesting and electronic collection efficiency; for instance, nanorod-like TiO_2 or ZnO could provide ordered straightforward nanochannels for electron transfer [12–14]. Planar PSCs do not include this nanostructured ETM (see Fig. 1(b)), and, if the ETM and HTM are exchanged, the device is called an “inverted PSC” (see Fig. 1(c)) [15–17]. The selective transporting ma-

Corresponding author: Min Guo E-mail: guomin@ustb.edu.cn

© University of Science and Technology Beijing and Springer-Verlag GmbH Germany, part of Springer Nature 2019

materials can not only transport the corresponding carriers but also block the carriers of opposite charge. The common ETMs include TiO_2 , ZnO , SnO_2 , [6,6]-phenyl-C61-butyric acid methyl ester (PCBM), C_{60} and so on [18–25], whereas HTMs include 2,2',7,7'-tetrakis-(*N,N*-di-*p*-methoxyphenylamine)-9,9'-spirobifluorene (Spiro-OMeTAD), poly[bis(4-phenyl)(2,4,6-trimethylphenyl)amine] (PTAA), poly(3-hexylthiophene-2,5-diyl) (P3HT), CuI , CuSCN , NiO , and poly(3,4-ethylenedioxythiophene)/poly(styrenesulfonate) (PEDOT:PSS), among others [21,26–27]. The perovskite layer is the core part of the device, and the perovskite film quality directly affects the device's PCE. The basic deposition methods of

perovskites include a single-step method and a two-step method. In the single-step method, the raw materials (e.g., lead halide, methylamine halide) are dissolved in the solvent (e.g., *N,N*-dimethylformamide (DMF)) to prepare the perovskite precursor solution; the solution is then spin-coated or doctor-blade-coated onto the substrate, followed by an annealing treatment [6,28]. In some reports, antisolvent dripping is used in the spin-coating process to ensure good perovskite morphology [29–31]. By contrast, in the two-step method, a PbI_2 film is prepared on the substrate first and the PbI_2 -coated substrate is subsequently reacted with $\text{CH}_3\text{NH}_3\text{I}$ (MAI), followed by an annealing treatment [32–34].

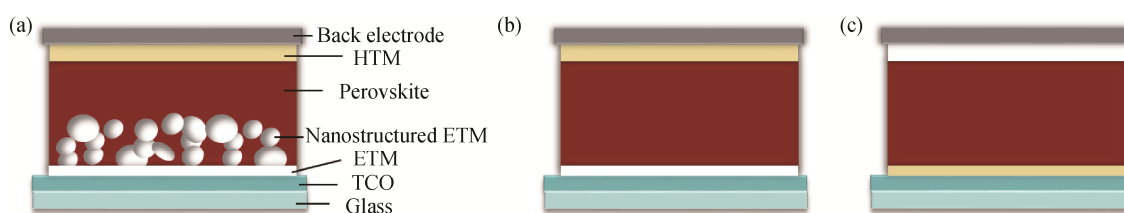


Fig. 1. Schematic of the basic structures of (a) mesoscopic, (b) planar, and (c) inverted PSCs.

Although PSCs can exhibit excellent PCEs, the poor stability of perovskite absorbers is a challenging problem. The chemical formula of the perovskite phase used in PSCs is ABX_3 , where A is a monovalent cation (e.g., Cs^+ , CH_3NH_3^+ , or $\text{CH}(\text{NH}_2)_2^+$), B is a divalent metal cation (e.g., Pb^{2+} or Sn^{2+}), and X is a halide ion (e.g., Cl^- , Br^- , or I^-) [35]. Perovskite materials will decompose quickly under moisture or heat [36–38]; thus, the lifetime of PSCs is much shorter than that of Si-based solar cells. In addition, most of the efficient PSCs have been fabricated with a lead halide [10–11,39–42], and Pb^{2+} , as a heavy-metal ion, is harmful to the environment and to human health. Therefore, the Pb^{2+} released from the unstable perovskites poses an environmental hazard, which is another huge obstacle to the commercialization of PSCs. Solutions such as optimizing the perovskite's composition [43–46], passivating the perovskite grain boundaries [47–49], and modifying the interfaces between the perovskite and carrier-transporting layers [50–52] have been used to prevent or retard perovskite degradation. However, these approaches are insufficient to enable the industrial application of PSCs. To produce low-toxicity PSCs with high efficiency, the most effective approach is to find a less toxic element to partially or fully substitute Pb in the devices.

In this review, we summarize some recent works on Pb-less and Pb-free perovskites for photovoltaic applications. The semiconductor properties and photovoltaic performance of the Pb-less and Pb-free perovskites are discussed systematically, and the merits and shortcomings of the perovskites prepared with different substitutions of Pb, such as

those substituted with group 14, 2, 13, and 15 elements and transition-metal elements are compared in detail. We emphasize that optimizing the perovskite composition, perovskite deposition methods, and the device structures are the most promising approaches to fabricating highly efficient, low-toxic, and stable PSCs in the future.

2. Design and application of lead-less and lead-free perovskite materials in PSCs

Generally, The crystal structure of ABX_3 perovskite-structured phases is determined by the Goldschmidt's tolerance factor t and octahedral factor μ :

$$t = (r_A + r_X) / \sqrt{2}(r_B + r_X) \quad (1)$$

$$\mu = r_B / r_X \quad (2)$$

where r_A , r_B , and r_X represent the radii of A, B, and X, respectively. To form an efficient three-dimensional (3D) perovskite structure, the radii of the three ions must meet the conditions $0.81 < t < 1.11$ and $0.44 < \mu < 0.90$ [21,53–54]. If the value of t is too small, the compound cannot form the perovskite structure; if the value of t is too large, the compound forms a low-dimensional perovskite structure. When the t value is between 0.89 and 1.0, the compound shows a stable cubic structure (see Fig. 2) because the lattice distortion is smaller than that associated with the octahedral or tetragonal structure. According to the tolerance factor and octahedral factor, the chemical composition of the perovskite structure has been constantly optimized to stabilize the pe-

rovskite crystal lattice [36,55–58]. Meanwhile, the two aforementioned empirical parameters can be used to predict the elements in the periodic table that are candidates for substituting Pb in the perovskite structure. Over the past few years, many research groups have studied the potential substitutions of Pb on the basis of theoretical calculations and experimental experiments, and the reported elements used to prepare Pb-less or Pb-free perovskites are summarized in Fig. 3. In the following sections, we will discuss these substitution works in detail.

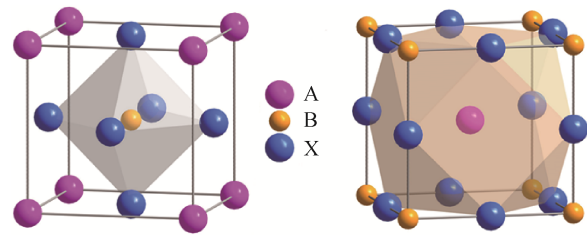


Fig. 2. Schematic of the cubic structure of perovskite. The B cation is surrounded by six X anions, forming a symmetric octahedron. The A cation is surrounded by 12 X anions, forming a cuboctahedron.

1																18			
2											13	14	15	16	17				
	Mg	3	4	5	6	7	8	9	10	11	12								
	Ca					Mn	Fe	Co	Ni	Cu	Zn		Ge						
	Sr								Pd				In	Sn	Sb				
	Ba										Hg		Pb	Bi					

Fig. 3. Periodic table showing elements reportedly substituted for Pb in the perovskite structure.

2.1. Group 14 elements

2.2.1. Sn substitution

As a suitable element to substitute Pb in the perovskite structure, the most obvious choice is Sn or Ge. Because Ge, Sn, and Pb are in the same main group, the three elements should have similar chemical properties. In 2014, Ogomi *et al.* [59] introduced Sn into the fabrication of PSCs for the first time. They prepared various Sn-substituted perovskite films via a single-step spin-coating method and investigated the change in the perovskite's optical properties and photovoltaic performance with increasing Sn content. They found that Sn substitution reduced the perovskite's optical bandgap and extended the absorption onset into the infrared region. When the Sn content was 50mol%, the band-edge wavelength was 1060 nm, showing a 260-nm red shift compared with that for the MAPbI₃ perovskite. To match the changed conduction-band minimum of the perovskite, a new HTM, poly(3-hexylthiophene-2,5-diyl) (P3HT), was used in the mesoscopic MAPb_xSn_{1-x}I₃-based PSC. However, the optimized MAPb_{0.5}Sn_{0.5}I₃-based PSC only achieved a PCE of 4.18%, and the 100% Sn-based PSC showed a PCE of 0%. X-ray photoelectron spectroscopy analysis demonstrated that the Sn²⁺ was easily oxidized to Sn⁴⁺, which led to

self-doping effect that increased charge combination in the perovskite and thus adversely affected device performance.

Noel *et al.* [60] fabricated MASnI₃-based mesoscopic PSCs with mesoscopic TiO₂ and Al₂O₃ substrates. Notably, the mesoscopic TiO₂-based device achieved a PCE of 6.4% and its open-circuit voltage (V_{oc}) of 0.88 V and short-circuit current density (J_{sc}) of 16.8 mA·cm⁻² were very similar to those of the reference MAPbI₃-based PSC. However, the device based on mesoporous Al₂O₃ showed a negligible PCE, suggesting that the as-prepared Sn-based perovskite film had a short carrier diffusion length. The authors estimated the carrier mobility and diffusion length of MASnI₃ to be 1.6 cm²·V⁻¹·s⁻¹ and 30 nm, respectively, and attributed the short diffusion length to recombination with self-doping carriers. Hao and co-workers [61] introduced Br into the MASnI₃ perovskite to engineer its bandgap (see Fig. 4 [61]). They dissolved the synthesized MASnI_{1-x}Br_x powder into DMF and then spin-coated the perovskite precursor solution onto the mesoporous substrate to prepare the MASnI_{1-x}Br_x films. The characterization results demonstrated that, with increasing x in MASnI_{3-x}Br_x, the perovskite's optical bandgap increased, and the PSC's incident photon-to-current efficiency (IPCE) onset showed a substantial blue shift. When $x = 2$, the PSC achieved the highest PCE of 5.73%.

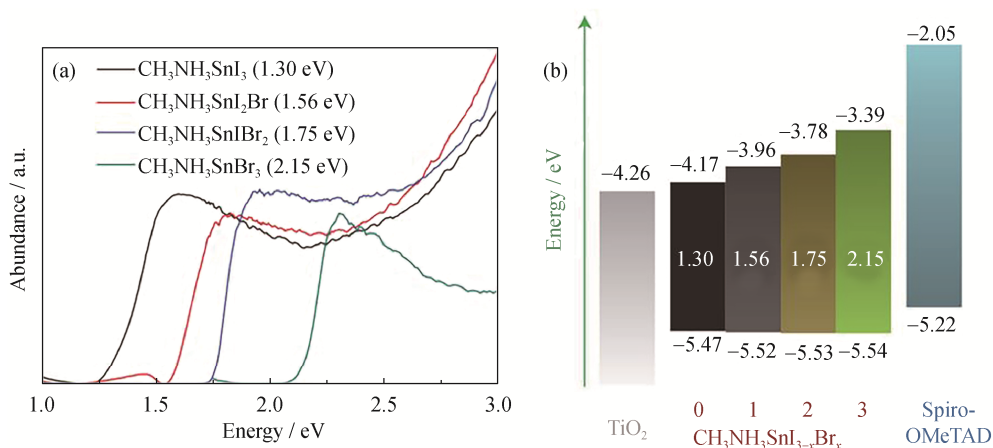


Fig. 4. Absorption spectra (a) and a schematic energy band (b) of the $\text{MASnI}_{3-x}\text{Br}_x$ ($x = 0, 1, 2, 3$) perovskites. Reprinted by permission from Springer Nature: *Nature Photonics*, Lead-free solid-state organic–inorganic halide perovskite solar cells, F. Hao, C.C. Stoumpos, D.H. Cao, R.P.H. Chang, and M.G. Kanatzidis, Copyright 2014.

Koh *et al.* [62] reported that SnF_2 could effectively slow the oxidation of Sn^{2+} and improve the film quality and stability of Sn-based perovskites. With this SnF_2 additive, they constructed an FASnI_3 -based mesoscopic PSC with a PCE of 2.1%. SnF_2 has since been widely applied to fabricate Sn-based PSCs. Liao *et al.* [63] fabricated a compact FASnI_3 perovskite film via an antisolvent-assisted single-step method, and the corresponding inverted PSC achieved a PCE of 6.22%. An illumination stability test of the encapsulated device showed that its PCE decreased only 5.8% from its initial efficiency within 30 d. The authors speculated that the perovskite deposition method and device structure were critical to the fabrication of highly efficient Pb-free PSCs.

Ke *et al.* [64] added ethylenediammonium {en} to the perovskite precursor solution and prepared a new perovskite material, {en} FASnI_3 . They found that en could effectively increase the bandgap of perovskite as a result of massive Schottky-type defects, and the {en} FASnI_3 -based PSC achieved a PCE of 7.14%. After a 1000-h aging process, the device with encapsulation retained 96% of its initial PCE, indicating that the incorporation of en improved device stability. Subsequently, the authors increase the PCE of {en} FASnI_3 -based PSC to 7.23% by using a novel material, tetrakis-triphenylamine (TPE), as the HTM [65].

Zhao *et al.* [66] prepared FA–MA mixed Sn-based perovskite films via an antisolvent-assisted single-step method and investigated the effect of organic-cation mixing on the optical properties and photovoltaic performance of Sn-based perovskite films. They found that increasing the FA content could improve the film morphology and modulate the perovskite's energy level. When 10mol% SnF_2 was added to the perovskite precursor solution, the resultant

$\text{FA}_{0.75}\text{MA}_{0.25}\text{SnI}_3$ -based inverted PSC exhibited a PCE of 8.12%. They attributed the improved performance to an enhancement of the device's V_{oc} through composition engineering.

Moreover, Yokoyama *et al.* [67] reported a vapor-assisted solution-process that could increase the Sn-based perovskite film coverage and thus overcome the device's short-circuit phenomenon. Xi *et al.* [68] fabricated a Sn-based PSC on a flexible substrate and achieved a PCE of 3.12%. Marshall *et al.* [69] fabricated a HTM-free CsSnI_3 -based PSC with a PCE of 3.56%. Ran *et al.* [70] used a mixed perovskite with a 2D–3D bulk heterojunction structure as light harvester and fabricated a Sn-based PSC with a PCE of 6.98%. Some other researchers found that replacing the organic cation with Cs^+ in the perovskite enabled the fabrication of an all-inorganic perovskite with high thermal stability [71], and they used $\text{CsSnI}_{3-x}\text{Br}_x$ as perovskite absorber to fabricate solar cells [72–78]. Obviously, the development of Pb-free PSCs has been showing a tendency toward diversification.

According to the aforementioned reports, we find that the PCEs of Sn-based PSCs are still much lower than those of Pb-based PSCs. Notably, the oxidation tendency of Sn^{2+} is a substantial roadblock for the enhancement of device's stability and PCE. Nevertheless, it has been revealed that partial substitution of Pb with Sn in the PSC can mitigate the oxidation of Sn^{2+} , and the PSC based on the Sn–Pb mixed perovskite could possess a better photovoltaic performance [59]. Zhu *et al.* [79] replaced 10mol% of Pb in the perovskite film with Sn and constructed a $\text{MASn}_{0.1}\text{Pb}_{0.9}\text{I}_3$ -based inverted PSC. They found that a dimethylsulfoxide (DMSO) vapor-assisted annealing treatment was beneficial to preparing a compact Sn–Pb mixed perovskite film with large and

smooth grains and that the device achieved a PCE of 10.25%. Zuo *et al.* [80] replaced partial PbCl_2 with SnCl_2 in the perovskite precursor solution to prepare a Pb-less PSC. Through a time-resolved scanning electron microscopy study of the perovskite growth, they found that Sn^{2+} induced a dynamic morphological modulation during the annealing process because of the effect of Sn^{2+} on nucleation and growth. This modulation promoted the formation of a highly covered perovskite film. When the Sn content was 15mol%, the better film morphology reduced charge recombination and improved carrier transport, thus increasing the inverted PSC's fill factor (FF). Meanwhile, the enhanced light absorption increased the short-circuit current density (J_{sc}). Finally, the device exhibited a maximum PCE of 10.1%.

Some researchers have found that, in the two-step spin-coating method, adding dimethyl sulfoxide (DMSO) to the $\text{PbI}_2/\text{SnI}_2$ precursor solution led to the formation of a “ $\text{PbI}_2\text{-DMSO-SnI}_2$ ” adduct, which was beneficial to preparing a compact perovskite film with a large grain size [81–83]. The 25mol% Sn-substituted PSC based on this deposition method could achieve a PCE of approximately 14%. In general, there are more defects at grain boundaries than in the grains. If the perovskite film has a larger grain size, fewer grain boundaries are formed, resulting in reduction of the defect density of the perovskite film. A lower defect density will reduce carrier recombination in the PSC, enhancing the device's PCE. Furthermore, Liu *et al.* [83] reported that the introduction of C_{60} as an additive to the $\text{PbI}_2/\text{SnI}_2$ solution could tune the perovskite crystallization and that the C_{60} at the grain boundaries exhibited a passivating effect, which decreased the trap-state density. The resultant $\text{MASn}_{0.25}\text{Pb}_{0.75}\text{I}_3$ -based inverted PSC with C_{60} additive demonstrated a higher PCE and a smaller hysteresis effect than a reference PSC. In addition, the C_{60} could prevent the penetration of moisture and oxygen, enhancing the device's stability in the ambient atmosphere.

The first principles calculations demonstrated that 50mol% Sn substitution for Pb in the perovskite could not only broaden the absorption region but also balance the electron- and hole-transporting properties and that the 50:50 (molar ratio) Sn–Pb mixed perovskite would exhibit better anti-oxygenation [84]. Therefore, a $\text{MASn}_{0.5}\text{Pb}_{0.5}\text{I}_3$ -based PSC should display enhanced photovoltaic performance in comparison with the analogous MAPbI_3 -based PSC. Hao *et al.* [85] investigated the optical properties of an Sn–Pb mixed perovskite ($\text{MASn}_x\text{Pb}_{1-x}\text{I}_3$) based on the alloyed perovskite solid solutions of $\text{MASn}_x\text{Pb}_{1-x}\text{I}_3$. They found that the perovskites' bandgaps did not show a linear trend (Ve-

gard's law) with increasing x value and that the $\text{MASn}_x\text{Pb}_{1-x}\text{I}_3$ perovskites exhibited a smaller bandgap than MASnI_3 when $x = 0.25, 0.5, \text{ or } 0.75$. Finally, the $\text{MASn}_{0.5}\text{Pb}_{0.5}\text{I}_3$ -based PSC showed a PCE (7.27%) lower than that of the MAPbI_3 -based one (8.31%); however, it had a broader IPCE onset and its J_{sc} reached $\sim 20 \text{ mA}\cdot\text{cm}^{-2}$. Li *et al.* [86] successfully prepared a flat and compact $\text{MASn}_{0.5}\text{Pb}_{0.5}\text{I}_3$ perovskite film via a two-step spin-coating method. Using this highly covered perovskite film, they fabricated an inverted PSC that exhibited an excellent PCE of 13.6%. Xu and co-workers [87] used ascorbic acid as an additive in the fabrication of $\text{FA}_{0.5}\text{MA}_{0.5}\text{Pb}_{0.5}\text{Sn}_{0.5}\text{I}_3$ -based PSCs. Ascorbic acid, as an antioxidant, retarded the oxidation of Sn^{2+} , and the resultant PSC achieved a PCE of 14.01%. Kapil *et al.* [88] speculated that interfacial engineering could improve the performance of the 50mol% Sn-substituted PSC (see Fig. 5 [88]). They prepared the Sn-substituted perovskite via an antisolvent-assisted single-step method and inserted a PCBM layer between C_{60} and $\text{FA}_{0.5}\text{MA}_{0.5}\text{Sn}_{0.5}\text{Pb}_{0.5}\text{I}_3$ perovskite to fabricate an inverted planar PSC. Interfacial traps in the PSC were reduced remarkably, the device's V_{oc} increased from 0.68 to 0.75 V, and the PCE reached 17.6%.

Lee and Kang [89] investigated the effect of Br substitution on the photovoltaic performance of the $\text{MASn}_{0.6}\text{Pb}_{0.4}\text{I}_3$ -based PSC. In their work, Br could improve the crystallinity and coverage of the perovskite. When the Br content was 40mol% in the perovskite, the carrier combination was effectively suppressed and the device achieved a PCE of 12.1%. Liao *et al.* [90] combined FASnI_3 with MAPbI_3 in different ratios in the perovskite precursor solution to investigate the effects of the MAPbI_3 content on the film-formation behavior, optical behavior, and carrier dynamics of the perovskite. They found that, when the mole ratio of FASnI_3 and MAPbI_3 was 6:4, the mixed perovskite exhibited a compact and uniform morphology, a broader absorption range, and a longer carrier lifetime compared with the FASnI_3 perovskite analog. The inverted PSC prepared with the $(\text{FASnI}_3)_{0.6}(\text{MAPbI}_3)_{0.4}$ perovskite achieved an excellent PCE of 15.08%. After the thickness of perovskite absorber was optimized, the device's PCE increased to 17.6% and the external quantum efficiencies in the wavelength range from 700 to 900 nm were greater than 70% [91]. Notably, in these works, the J_{sc} values of the mixed perovskite devices were greater than $26 \text{ mA}\cdot\text{cm}^{-2}$, which is higher than those of highly efficient Pb-based PSCs [11,92–93], demonstrating the advantage of the Sn–Pb mixed perovskite's wide absorption range.

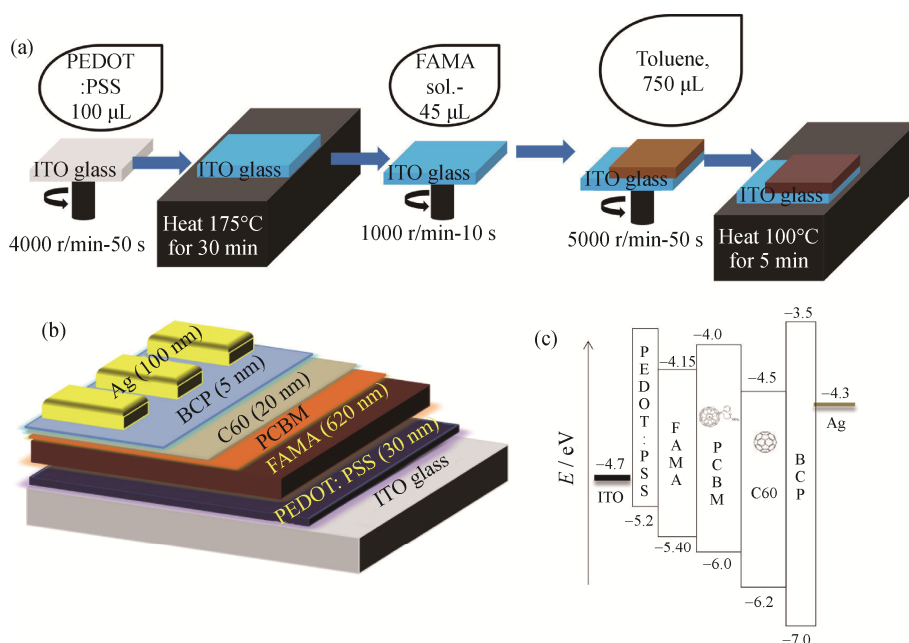


Fig. 5. (a) Schematic of the perovskite film, (b) schematic structure of the constructed device, and (c) schematic energy level of the different layers in the PSC. Reprinted with permission from Ref. [88]. Copyright 2018 American Chemical Society.

Tavakoli and co-workers [94] prepared various Sn–Pb mixed perovskites via the reaction between Sn–Pb alloy precursors and MAI vapor in a chemical vapor deposition process. When the Sn content was 62wt%, the as-constructed PSC achieved a PCE of 14.04%. Tsai *et al.* [95] fabricated HTM-free carbon-based mesoscopic solar cells with Sn–Pb mixed perovskites. They substituted PbI_2 with SnCl_2 or SnI_2 in the perovskite precursor solution to synthesize the $\text{MASn}_y\text{Pb}_{1-y}\text{I}_{3-x}\text{Cl}_x$ perovskite, and they found that the incorporation of SnCl_2 modified the lattice structure, resulting in optical and optoelectronic properties that included an anomalous transition. When the Sn content was increased, SnCl_2 -doped and SnI_2 -doped perovskite presented different variations of the bandgaps and band energy. With the introduction of SnF_2 additive in the precursor solution, the $\text{MASn}_{0.75}\text{Pb}_{0.25}\text{I}_{3-x}\text{Cl}_x$ -based PSC achieved a PCE of 4.35%, which showed a slight degradation in a N_2 -filled glovebox after 4000 h. When an NiO layer was added as a HTM, the device's efficiency increased to 5.13%.

The results related to the aforementioned Sn-containing PSCs are summarized in Table 1. The results in the table show that the device structures and perovskite deposition methods of Pb-based PSCs are also applicable to Sn-containing PSCs. Currently, the efficiency and device stability of fully Sn-based PSCs remain unsatisfactory. The oxidation of Sn^{2+} , which will induce the recombination of self-doping carriers, is difficult to control. This problem is the single biggest obstacle to the enhancement of the per-

formance of the Sn-based PSC. Compared with the fully Sn-based perovskites, the Sn–Pb mixed perovskites demonstrate better film controllability; that is, a compact, highly covered and defect-less Sn–Pb mixed perovskite film can be prepared more easily. More importantly, after the Sn-to-Pb ratio is adjusted, the perovskite film can exhibit a wider absorption range than the fully Pb-based and fully Sn-based perovskite films. Therefore, the Sn–Pb mixed PSCs exhibit better photovoltaic performance than Sn-based devices. Despite these advantages, the development of Sn-containing PSCs severely lags that of Pb-based PSCs. Future efforts should be devoted to enhancing the film quality (e.g., passivating grain boundaries, enlarging the size of perovskite grains), reducing interfacial traps (e.g., interfacial engineering), and preventing the oxidation of Sn^{2+} (e.g., utilizing additives and encapsulation).

2.2.2. Ge substitution

Krishnamoorthy *et al.* [96] explored the possibility of substituting Pb with Ge substitution in the PSCs on the basis of density of states (DOS) calculations and experimental explorations. They found that Ge-based perovskites could be synthesized and that the perovskite's optical bandgap could be tuned via the radius of the cation at the A-site. For Cs^+ , MA^+ , and FA^+ , whose radii increase in sequence, the bandgaps of the corresponding CsGeI_3 , MAGeI_3 , and FAGeI_3 perovskites are 1.63, 2.0, and 2.35 eV, respectively. However, the Ge-based solar cells showed poor PCEs ($\leq 0.2\%$) because of the poor morphology of the perovskite films and

the oxidation of Ge^{2+} , akin to that of Sn^{2+} . Kopacic *et al.* [97] optimized the chemical composition of Ge-based perovskite

and fabricated a $\text{MAGeI}_{2.7}\text{Br}_{0.3}$ -based inverted PSC with a PCE of 0.57%.

Table 1. Reported Sn-doped and Sn-based PSCs

Sn content / mol%	Device structure	Perovskite deposition method	PCE / %	Reference
10	ITO/PEDOT:PSS/MASn _{0.1} Pb _{0.9} I ₃ /PCBM/C ₆₀ /BCP/Al	Two-step spin-coating method	10.25	[79]
15	ITO/PEDOT:PSS/MASn _{0.15} Pb _{0.85} I ₃ /PCBM/C ₆₀ -bis/Ag	Single-step method	10.10	[80]
25	ITO/PEDOT:PSS/MASn _{0.25} Pb _{0.75} I ₃ /PCBM/BCP/Ag	Two-step spin-coating method	14.12	[81]
25	ITO/PEDOT:PSS/MASn _{0.25} Pb _{0.75} I ₃ /PCBM/BCP/Ag	Two-step spin-coating method	14.01	[82]
25	FTO/PEDOT:PSS/MASn _{0.25} Pb _{0.75} I ₃ /PCBM/BCP/Ag	Two-step spin-coating method	13.90	[83]
50	FTO/compact TiO ₂ /mesoporous TiO ₂ /MASn _x Pb _{1-x} I ₃ /P3HT/Ag/Au	Single-step method	4.18	[59]
50	ITO/PEDOT:PSS/MASn _{0.5} Pb _{0.5} I ₃ /C ₆₀ /BCP/Ag	Two-step spin-coating method	13.6	[86]
50	ITO/PEDOT:PSS/FA _{0.5} MA _{0.5} Sn _{0.5} Pb _{0.5} I ₃ /PCBM/bis-C ₆₀ /Ag	Single-step method (antisolvent dripping)	14.01	[87]
50	ITO/PEDOT:PSS/FA _{0.5} MA _{0.5} Sn _{0.5} Pb _{0.5} I ₃ /PCBM/C ₆₀ /BCP/Ag	Single-step method (antisolvent dripping)	17.60	[88]
60	ITO/PEDOT:PSS/MASn _{0.6} Pb _{0.4} I _{2.6} Br _{0.4} /PCBM/Ag	Single-step method (drop casting)	12.10	[89]
60	ITO/PEDOT:PSS/(FASnI ₃) _{0.6} (MAPbI ₃) _{0.4} /C ₆₀ /BCP/Ag	Single-step method (antisolvent dripping)	15.08	[90]
60	ITO/PEDOT:PSS/(FASnI ₃) _{0.6} (MAPbI ₃) _{0.4} /C ₆₀ /BCP/Ag	Single-step method (antisolvent dripping)	17.60	[91]
74	FTO/compact TiO ₂ /MASn _x I ₃ /Spiro-OMeTAD/Au	Alloying technique	14.04	[94]
75	FTO/TiO ₂ /Al ₂ O ₃ /NiO/C	Single-step method (drop casting)	5.13	[95]
100	FTO/compact TiO ₂ /mesoporous TiO ₂ /MASnI ₃ /Spiro-OMeTAD/Au	Single-step method	6.40	[60]
100	FTO/compact TiO ₂ /mesoporous TiO ₂ /MASnI ₃ /Spiro-OMeTAD/Au	Single-step method	5.73	[61]
100	ITO/PEDOT:PSS/FASnI ₃ /C ₆₀ /BCP/Ag	Single-step method (antisolvent dripping)	6.22	[63]
100	(flexible) ITO/PEDOT:PSS/FASnI ₃ /C ₆₀ /BCP/Ag	"Multichannel interdiffusion"	3.12	[68]
100	FTO/compact TiO ₂ /mesoporous TiO ₂ /MASnI ₃ /PTAA/Au	"Vapor-assisted solution-process"	1.86	[67]
100	FTO/compact TiO ₂ /mesoporous TiO ₂ /FASnI ₃ /TPE/Au	Single-step method	7.23	[65]
100	ITO/LiF/PEDOT:PSS/PEA ₂ FA _{n-1} Sn _n I _{3n+1} /PCBM/C ₆₀ /BCP/Ag	"Multichannel interdiffusion"	6.98	[70]
100	ITO/PEDOT:PSS/FA _{0.75} MA _{0.25} SnI ₃ /C ₆₀ /BCP/Ag	Single-step method (antisolvent dripping)	8.12	[66]

Note: BCP—Bathocuproine.

Using first-principle calculations, Wang *et al.* [98] investigated the electronic and optical properties of MAPbI₃, MASnI₃, MAGeI₃, and MASrI₃. They found that the lattice distortion induced by the metal ions whose radii are smaller than that of Pb²⁺ led to a diminished *p-p* transition and a larger carrier effective mass. The metal ions' outer *ns*² electrons were critical to the perovskites' electronic and optical properties. Therefore, the simple replacement of Pb with Sn, Ge, or Sr did not enhance the devices' PCE. It was suggested that alternative metal or metallic clusters should have the same ionic radius and outer *ns*² electron configuration as Pb²⁺.

In summary, the construction of Ge-based PSCs appears to be more difficult than those of Pb- and Sn-based PSCs because of the poor stability of Ge-based perovskites; and attempts to prepare Ge-based devices are correspondingly rare. More attention should be devoted to the compositional

engineering and development of selective contacts for Ge-containing PSCs. Ge–Pb mixed perovskites, for example, might behave better.

2.2. Group 2 elements

Alkaline-earth-metal cations, belonging to group 2, have the same valence (+2) as Pb²⁺ and are more stable than Sn²⁺ and Ge²⁺. Notably, the radii of Sr²⁺ and Pb²⁺ are nearly identical [99]. Jacobsson *et al.* [100] studied the property of MASrI₃ by coupled cluster and density functional theory (DFT) calculations. Their calculation results showed that strontium halides and lead(II) chloride had similar bonding patterns and that MASrI₃ could form a stable phase irrespective of the electronegativity difference between Sr²⁺ and Pb²⁺ ions. However, the optical bandgap of MASrI₃ was estimated to be 3.6 eV, suggesting that MASrI₃ could not function as a light absorber in PSCs. Pazoki and co-workers [99]

explored the electronic properties of MACaI_3 , MASrI_3 , and MABaI_3 using DFT calculations and estimated bandgaps of 2.95, 3.6, and 3.3 eV, respectively, for the three compounds. They speculated that the alkaline-earth-based perovskite materials were more appropriate for use as selective contacts than for use as light absorbers.

Some research groups have used PbCl_2 and MAI as raw materials and have partially replaced PbCl_2 with an alkaline-earth metal halide in the perovskite precursor solution to fabricate Pb-less planar PSCs via a single-step perovskite deposition procedure. For instance, Wu and co-workers [101] replaced some PbCl_2 in the precursor solution with SrI_2 or BaI_2 to study the effect of the Sr or Ba dopant on the device's photovoltaic performance. They found that both the Sr and the Ba dopants would reduce the coverage of the perovskite film, resulting in a decreasing device PCE with increasing Sr or Ba content. When 10mol% of the Pb was replaced, the Ba-doped PSC achieved a better PCE of 9.7% than the PSC with the Sr-doped analog. They later replaced some of the PbCl_2 with CaI_2 to prepare Ca-doped perovskite films and PSCs [102]. The results showed that the Ca dopant could reduce the bandgap and extend the absorption to the visible range; the 1mol% Ca-doped PSC achieved a higher PCE of 12.9%. Zhang *et al.* [103] prepared a Ba-doped perovskite film by replacing the PbCl_2 in the precursor solution with BaCl_2 . They found that the Ba dopant could induce a slight upshift in the conduction-band minimum. For the device, 2mol% Ba dopant enhanced the V_{oc} and the J_{sc} and an excellent PCE of 17.4% was achieved. Chan and co-workers [104] replaced PbCl_2 in the precursor solution with MgI_2 , CaI_2 , SrI_2 , or BaI_2 and investigated the effects of four dopants on the morphology and photovoltaic property of perovskites. Only the Ba dopant improved the coverage of the perovskite film. Moreover, the Ba dopant could enhance the crystallinity, absorption behavior, and charge separation efficiency of the perovskites; the device fabricated with 3mol% Ba achieved a record PCE of 14.9%. In addition, the Ba-doped PSC showed a better stability than the pristine PSC.

Shai *et al.* [105] chose the two-step spin-coating method to prepare Sr-doped perovskite films, and they found that SrCl_2 substitution can influence the energy level of perovskite and increase the defect density and exciton binding energy of perovskite. The planar PSC fabricated using a perovskite with 5mol% SrCl_2 achieved a maximum V_{oc} of 1.11 V because of the up-shifted conduction-band maximum and the PCE reached 16.3%. Lau *et al.* [106] introduced SrI_2 into the preparation of a CsPbI_2Br -based PSC, and they found that the SrI_2 substitution lowered the conversion tempera-

ture of the fully inorganic perovskite. In their work, an annealing temperature of 100°C was sufficient to form the $\text{CsPb}_{0.98}\text{Sr}_{0.02}\text{I}_2\text{Br}$ perovskite film, and the resultant PSC achieved a PCE of 11.3% and better thermal stability than the unsubstituted CsPbI_2Br -based PSC. Moreover, in some reports, SrI_2 and SrCl_2 were used as additives in the precursor solution to prepare perovskite films, and the device's charge recombination could be effectively suppressed, increasing the PCE to more than 15% [107–108].

From the aforementioned works, we find that alkaline-earth metal salts influence the film formation and optical properties of perovskite and that substitution at a low level enhances the photovoltaic performance of PSCs; however, the major contributor to device performance is Pb. Thus, other elements beyond alkaline-earth metals are needed to further increase the substitution amount of Pb.

2.3. Transition-metal elements

Like alkaline-earth metals, transition metals are also abundant in the Earth's crust. In addition, many transition metals' divalent cations satisfy the requirements for the tolerance factor and octahedral factor, with the exception of metal cations with strong reducibility or small ion radii. Some researchers have attempted to use Fe^{2+} [109], Mn^{2+} [110], Cu^{2+} [111–113], and Pd^{2+} [114] as Pb^{2+} substitutes to prepare Pb-free perovskites; however, the resultant compounds often show a 2D perovskite structure, which is undesirable for highly efficient PSCs. Therefore, to retain the 3D perovskite structure, partial substitution with transition metals appears to be a more reasonable approach.

Frolova *et al.* [115] studied the effects of a series of metal-ion substitutions on the photovoltaic performance of MAPbI_3 -based PSCs. They replaced 10mol% PbI_2 in the MAPbI_3 precursor solutions with different metal iodides (AgI , CuI , CdI_2 , BiI_3 , CoI_2 , NiI_2 , FeI_2 , ZnI_2 , and HgI_2) and fabricated the Pb-less PSCs via an antisolvent-assisted single-step method. With the exception of HgI_2 , the metal iodides decreased the PCE of the device. Hg^{2+} , however, is also a toxic metal ion that cannot be used in industrial production. Jahandar *et al.* [116] used CuBr_2 as a substitute for PbI_2 in the perovskite precursor solution and investigated the effects of various CuBr_2 concentrations on the film formation, electronic properties, and photovoltaic properties of the perovskite. They found that CuBr_2 and DMSO could form a $\text{CuBr}_2\text{-(DMSO)}_2$ adduct in the perovskite precursor film under antisolvent dripping. The $\text{CuBr}_2\text{-(DMSO)}_2$ adduct would translate into a liquid phase during the annealing treatment, which facilitated the formation of a perovskite film with large grains (see Fig. 6 [116]). At the same time,

Cu doping could induce an increase of the carrier density, resulting in improved film conductivity. When the CuBr_2 concentration in the perovskite solution was 5mol%, the J_{sc} and fill factor (FF) of the resultant inverted PSC were enhanced and a considerable PCE of 17.09% and better air stability were achieved. Jin *et al.* [117] found that the addition of Zn in the perovskite precursor could influence the nucleation and subsequent crystal growth processes, and a

ZnCl_2 dopant was beneficial for the formation of perovskite film with large grains in the antisolvent-assisted single-step method. After the optimization of the ZnCl_2 concentration, the 3mol% ZnCl_2 -substituted planar PSC achieved a higher PCE of 18.2% and showed a better stability. This improved performance was ascribed to the enlarged grain size, fully covered morphology, and decreased carrier recombination induced by the ZnCl_2 substitution.

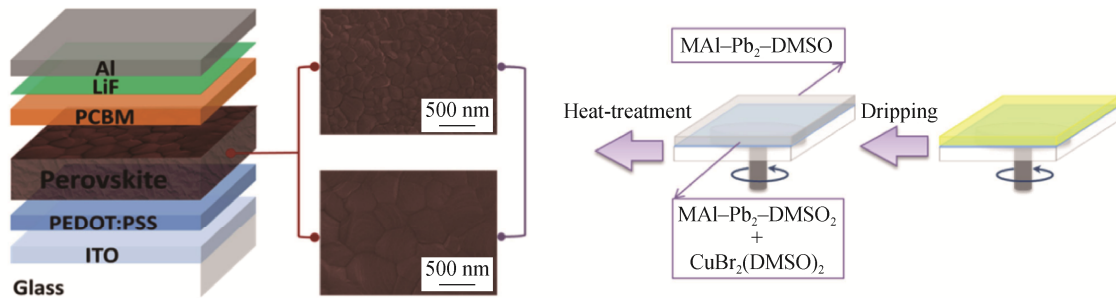


Fig. 6. Schematic of the device architecture of $\text{MAI}(\text{PbI}_2)_{1-x}(\text{CuBr}_2)_x$ planar hybrid perovskite solar cells with architecture ITO/PEDOT:PSS/perovskite/PCBM/LiF/Al. Reprinted from *Nano Energy*, 27, M. Jahandar, J.H. Heo, C.E. Song, K.-J. Kong, W.S. Shin, J.-C. Lee, S.H. Im, and S.-J. Moon, Highly efficient metal halide substituted $\text{CH}_3\text{NH}_3\text{I}(\text{PbI}_2)_{1-x}(\text{CuBr}_2)_x$ planar perovskite solar cells, 330-339, Copyright 2016, with permission from Elsevier.

Klug *et al.* [118] assessed the substitution feasibility of nine transition-metal species (Co, Cu, Fe, Mg, Mn, Ni, Sn, Sr, and Zn) for Pb-less PSCs. They replaced the lead acetate ($\text{Pb}(\text{Ac})_2$) in the perovskite precursor solution with these nine metal acetates or iodides to prepare the mixed perovskite and investigated the changes in the optical and photovoltaic properties caused by the substitutions. For most of the nine metal substitutions, the inverted PSCs were found to maintain an acceptable efficiency when the substitution content was less than 6mol%. However, when Fe was introduced into the perovskite, the device's PCE decreased to a relatively low level. The Sn-substituted PSCs maintained device efficiency even when the substitution level reached 25mol%. Notably, partially Co-substituted PSCs displayed enhanced photovoltaic performance, and a PCE of 17.2% was obtained for the PSC with a Pb:Co molar ratio of 63:1. With the increasing Co content, the perovskite's crystal structure transformed from cubic to tetragonal phase at room temperature. Likewise, the Co substitution tuned the Fermi energy level and valence-band edge without changing the bandgap of the perovskites, which facilitated a better energy level matching between the perovskite and PEDOT:PSS when the Pb:Co molar ratio was 63:1; thus, the device's V_{oc} was increased to 1.08 V. In addition, they speculated that Mg^{2+} , Mn^{2+} , Ni^{2+} , and Zn^{2+} may behave similarly to Co^{2+} in the PSCs because of their similar ionic radii, air stability as divalent ions, and slight influence on the device's photovol-

taic performance at low doping levels.

Because Sn^{2+} is not stable in the ambient atmosphere, the balance between device efficiency and Sn^{2+} content in the perovskite is a confusing problem. Li *et al.* [119] partially replaced PbI_2 with SnI_2 and CuBr_2 to synthesize Pb-Sn-Cu ternary PSCs via an antisolvent-assisted single-step method. Their findings showed that the introduction of Sn^{2+} widens the perovskite's absorption range but worsens the film quality. By contrast, the introduction of Cu^{2+} improved the film quality of the Sn-containing perovskite and reduced the trap density at grain boundaries without affecting the absorption. Thus, a high PCE of 21.08% was obtained for the $\text{MAPb}_{0.9}\text{Sn}_{0.05}\text{Cu}_{0.05}\text{I}_{2.9}\text{Br}_{0.1}$ -based inverted PSC because of the synergistic effect induced by Sn^{2+} and Cu^{2+} .

Although some transition metals (e.g., Cu and Zn) have successfully been used in photovoltaic devices such as $\text{CuIn}_x\text{Ga}_{1-x}\text{Se}_2$ (CIGS) [120] and $\text{Cu}_2\text{ZnSnS}_4$ (CZTS) [121-122] solar cells, they could only substitute less than 10mol% of the Pb in highly efficient PSCs, similar to substitution limits of the alkaline-earth metals. To further increase the substitution level of Pb, additional theoretical calculations are needed to deeply understand the energy-band construction of transition-metal-substituted 3D perovskites and deduce an appropriate chemical composition. In addition, optimization of the perovskite deposition method is also needed to suppress charge recombination.

2.4. Group 13 and 15 elements

In the previous sections, we mentioned the importance of Pb 6s electrons to the perovskite bandgap. Group 15 elements, such as Bi and Sb, can provide these extranuclear electrons, and Sb or Bi can be substituted into the perovskite structure without changing the 3D structure and forming n-type dopants because of the larger valence electron number of Sb 5p³ than that of Pb 6p² [123]. Oku *et al.* [124] first substituted PbI₂ with SbI₃ in the perovskite precursor solution to prepare a lead-less PSC via a single-step method. They found that Sb substitution could increase the perovskite's lattice constant and suppress the formation of excess PbI₂. When the Sb content increased from 0mol% to 3mol%, the mesoscopic PSC's PCE increased from 6.37% to 8.47%. Afterwards, Zhang *et al.* [123] prepared various Sb-doped perovskite films by replacing PbCl₂ with SbI₃ in the precursor solution and investigated the effects of Sb doping on the optical properties and photovoltaic performance of perovskite films. In their work, with increasing Sb content, the compound's absorption onset showed a blue shift, the optical bandgap increased from 1.55 to 2.06 eV, and the n-type doping of Sb up-shifted the perovskite's quasi-Fermi energy level and improved the electron transfer efficiency in the PSCs. When the Sb content was 1mol%, the device achieved an enhanced PCE of 15.6%. To increase the Sb doping content and control the morphology of Sb-substituted perovskite, Chatterjee *et al.* [125] used a two-step method to fabricate Sb-substituted inverted PSCs. After optimizing the deposition method of perovskite, they increased the Sb content to 8mol%; the corresponding device delivered a considerable V_{oc} of 1.13 V and a PCE of 12.8%.

The all-inorganic CsPbI₃-based PSCs exhibit better stability than the organic-inorganic hybrid PSCs; however, the highly efficient black phase (α -CsPbI₃) can easily degrade to the unwanted yellow phase (δ -CsPbI₃) [126]. Hu *et al.* [127] found that Bi³⁺ could suppress formation of the yellow phase and decrease the conversion temperature of the black phase to 100°C. They partially replaced PbI₂ with BiI₃ in the perovskite precursor solution and prepared a perovskite film via a single-step spin-coating method. When the Bi content was 4mol%, the resultant planar PSC achieved a PCE of 13.21% and maintained 68% of its initial efficiency after exposure in the ambient air for 168 h.

Indium (In), as a group 13 element, can also be substituted for Pb in the perovskite structure. Wang *et al.* [128] reported that InCl₃ could improve the crystallization quality of perovskite films. In their work, the introduction of InCl₃ increased the perovskite crystal orientation, which facilitated charge transport and, hence, enhanced device performance.

When the InCl₃ content was 15mol%, a high PCE of 17.55% was obtained for the Pb-In mixed PSC.

Unlike divalent cations, trivalent cations substituted at high concentrations will result in the compound losing its highly efficient 3D perovskite structure, although Pb-free PSCs prepared using these low-dimensional perovskites have been reported [129–139]. However, compared with 3D-structured perovskite, the low-dimensional structure results in a high exciton binding energy and a low carrier mobility; thus, the device's PCE is often less than 2%. The valence difference between Pb²⁺ and trivalent cations (Bi³⁺, Sb³⁺, In³⁺) clearly limits the extent to which perovskite Pb can be substituted.

2.5. Double perovskites

As previously discussed, to meet the requirements of tolerance factor and valence conservation, two divalent metal ions (e.g., Sn²⁺ and Pb²⁺) can be used to synthesize mixed perovskites. Why not replace the two divalent metal cations with a monovalent cation (e.g., K⁺, Ag⁺, or Cu⁺) and a trivalent cation (e.g., Bi³⁺ or Sb³⁺) to prepare Pb-free perovskites (see Fig. 7)? A new type of material called “double perovskites,” which is based on this design idea, has recently emerged. Slavney *et al.* [140] used equimolar amounts of Ag⁺ and Bi³⁺ as substitutes for toxic Pb²⁺ and synthesized Cs₂AgBiBr₆ with a 3D double-perovskite structure. The Cs₂AgBiBr₆ compound showed an indirect bandgap of 1.95 eV and a photoluminescence (PL) lifetime of approximately 660 ns. A comparison of the PL decay of both single-crystalline and powdered samples revealed that the Cs₂AgBiBr₆ compound had a high defect tolerance. Furthermore, the compound showed better heat and moisture stability than the MAPbI₃ perovskite. These traits demonstrate the potential of Cs₂AgBiBr₆ perovskite for photovoltaic applications. McClure *et al.* [141] synthesized Cs₂AgBiCl₆ and Cs₂AgBiBr₆ via the solid-state method and a solution method, respectively. Both compounds showed a cubic double-perovskite structure. Diffuse reflectance measurements indicated that the optical bandgaps of Cs₂AgBiCl₆ and Cs₂AgBiBr₆ were approximately 2.77 and 2.19 eV, respectively. The DOS calculation results demonstrated that the perovskite valence-band edge was characterized as the filled halogen 3p/4p states and that the conduction-band edge was defined as the antibonding Ag 5s and Bi 6p states. Furthermore, both the Cs₂AgBiCl₆ and Cs₂AgBiBr₆ perovskites were stable under ambient atmosphere. Volonakis *et al.* [142] combined theoretical calculations and experiments to study a series of compounds in the double-perovskite family based on group 15 metal ions (Bi³⁺, Sb³⁺) and noble-metal ions

(Ag⁺, Au⁺, Cu⁺). Their calculation results showed that the double perovskites possess highly tunable optical bandgaps and carrier effective masses. The authors predicted that all of the members of the double-perovskite family were indirect-gap semiconductors. Meanwhile, they synthesized a

Cs₂BiAgCl₆ compound with a face-centered cubic structure, and optical characterization demonstrated that the compound had an indirect gap. In addition, Wei *et al* synthesized MA₂KBiCl₃ perovskite with an optical bandgap of 3.04 eV [143] and MA₂AgBiBr₃ perovskite with a bandgap of 2.02 eV [144].

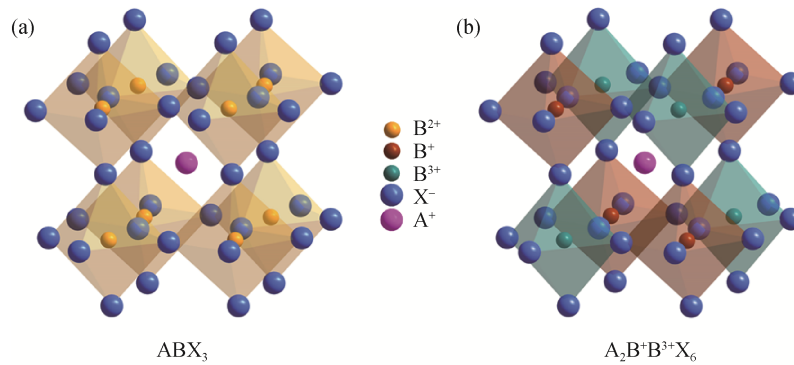


Fig. 7. Schematic crystal structure of the traditional perovskite (a) and double perovskites (b).

Although some single crystals and powders in the double-perovskite family have been synthesized, they could not be used in film-based PSCs. Greul *et al.* [145] successfully prepared a Cs₂AgBiBr₆ film and constructed a Cs₂AgBiBr₆-based mesoscopic PSC for the first time. They found that a high-temperature annealing treatment was necessary for complete conversion of the perovskite and that a preheating treatment was beneficial for enhancing the perovskite's optical properties. The resultant perovskite film exhibited a bandgap of 2.21 eV, consistent with a previous report [141]. The Cs₂AgBiBr₆-based PSC achieved a V_{oc} greater than 1 V and a PCE of approximately 2.5%; more importantly, the device showed greater illumination and air stability than the MAPbI₃-based PSC.

Ning *et al.* [146] constructed a Cs₂AgBiBr₆-based planar PSC with TiO₂ as the ETM. Because of the large-sized perovskite grains, the grain boundaries and carrier recombination were decreased and the double-perovskite film's carrier diffusion length reached 110 nm. The device achieved a PCE of 1.22%. Wu *et al.* [147] dissolved Cs₂AgBiBr₆ powder into DMSO to prepare a perovskite precursor solution. They prepared a compact perovskite film using a low-pressure-assisted spin-coating procedure. The resultant PSC with SnO₂ as the ETM and P3HT as the HTM achieved a PCE of 1.44%. Gao *et al.* [148] found that isopropanol dripping promoted the formation of smooth and uniform perovskite films with micro-sized grains. They fabricated an inverted Cs₂AgBiBr₆-based PSC with a PCE of 2.23% ($V_{oc} = 1.01$ V) via an antisolvent-assisted single-step method, and the efficiency only slightly decreased within 10 d in the

ambient air (25°C, 50% RH).

As a new family, double perovskites possess a better stability than the traditional organic–inorganic hybrid perovskites, but they haven't exhibit a considerable photovoltaic performance, and only Cs₂AgBiBr₆ was applied to construct devices at present. This is mainly ascribed to the wide indirect bandgaps. Fortunately, the double perovskite with a direct bandgap could be prepared by changing the chemical composition; for instance, Cs₂InAgCl₆ has a direct bandgap [149]. Therefore, more attempts are needed to modify the bandgap and carrier mobility of double perovskites.

3. Conclusion and outlook

After rapid development over several years, the exploration of PSCs has entered a buffer period. Researchers are beginning to devote more attention to the commercialization of devices, where the stability and toxicity of PSCs are the most important issues. In the past few years, numerous efforts have been made to seek for a suitable candidate of Pb to fabricate Pb-less or Pb-free PSCs. Sn, as group 14 element akin to Pb, has become a most promising substitution for Pb. Sn substitution can not only lower the toxicity of PSCs but also adjust the optical bandgap and, hence, improve the light-harvesting performance of perovskite. More importantly, almost all of deposition methods of perovskites and device structures for the Pb-based PSCs can be used to fabricate Sn-containing PSCs. However, the most efficient fully Sn-based PSC shows a PCE of only 8.12%, which is much lower than the PCEs of Pb-based PSCs. The greatest

problem associated with Sn-based PSCs is the oxidation tendency of Sn^{2+} , which induces a self-doping effect and thereby increases charge recombination in the perovskite. Measures such as interfacial engineering, the introduction of SnF_2 additive, and device encapsulation have been used to retard the oxidation; however, the final effects are finite. Meanwhile, another group 14 element, Ge, shows a more unsatisfactory performance because of the same oxidation issue. The partial substitution for Pb appears to be more feasible. The bandgap transition of Sn–Pb mixed perovskites does not show a linear trend (Vegard's law) with increasing Sn content, and the 50mol%–60mol% Sn-substituted perovskite exhibits the broadest absorption region. At the same time, the presence of Pb^{2+} in the perovskite can slow the oxidation of Sn^{2+} . Until now, Sn–Pb mixed PSCs can exhibit a PCE of 17.6% in devices with a Sn content of 60mol%.

To maintain or enhance the photovoltaic performance of PSCs, the substitution amounts of group 2 elements, transition-metal elements, and group 13 and 15 elements are kept at low levels. Although these species can influence the film formation, optical bandgap, and defect density of perovskites, the primary contribution to device photovoltaic performance originates from Pb. In fact, the incorporation state of these metals with Pb-based perovskite is still uncertain because of the limited characterization methods. Moreover, to deeply understand the energy-band construction of alkaline-earth-metal or transition-metal-substituted 3D perovskites, more theoretical calculations should be conducted.

To date, the PCEs of the PSCs fabricated with double perovskites have been less than 3% because most of the double perovskites are indirect-bandgap semiconductors, which adversely affects their photovoltaic performance. However, double perovskites possess better air and moisture stability compared with traditional organic–inorganic hybrid perovskites. An effective way to modify the energy bands of double perovskites is to adjust their element composition, and the new double perovskites with a direct bandgap will appear soon.

In conclusion, each Pb-free or Pb-less perovskite material has its attractive features. According to the present reports, the high PCEs of devices are influenced by numerous physical or chemical factors. We propose that future research toward environmentally friendly perovskite materials should be focused on the design of the elemental composition, the deposition method, and interfacial engineering. Given the hard work of an increasing number of PSC researchers, we believe that the commercialization of PSCs, and various highly efficient Pb-free or Pb-less PSC modules, will emerge in the near future.

Acknowledgements

This work was financially supported by the National Natural Science Foundation of China (Nos. 51572020 and 51772023).

References

- [1] A. Kojima, K. Teshima, Y. Shirai, and T. Miyasaka, Organometal halide perovskites as visible-light sensitizers for photovoltaic cells, *J. Am. Chem. Soc.*, 131(2009), No. 17, p. 6050.
- [2] K. Tanaka, T. Takahashi, T. Ban, T. Kondo, K. Uchida, and N. Miura, Comparative study on the excitons in lead-halide-based perovskite-type crystals $\text{CH}_3\text{NH}_3\text{PbBr}_3$, $\text{CH}_3\text{NH}_3\text{PbI}_3$, *Solid State Commun.*, 127(2003), No. 9-10, p. 619.
- [3] T. Baikie, Y.N. Fang, J.M. Kadro, *et al.*, Synthesis and crystal chemistry of the hybrid perovskite $(\text{CH}_3\text{NH}_3)\text{PbI}_3$ for solid-state sensitized solar cell applications, *J. Mater. Chem. A*, 1(2013), No. 18, p. 5628.
- [4] C.C. Stoumpos, C.D. Malliakas, and M.G. Kanatzidis, Semiconducting tin and lead iodide perovskites with organic cations: Phase transitions, high mobilities, and near-infrared photoluminescent properties, *Inorg. Chem.*, 52(2013), No. 15, p. 9019.
- [5] S.Y. Sun, T. Salim, N. Mathews, *et al.*, The origin of high efficiency in low-temperature solution-processable bilayer organometal halide hybrid solar cells, *Energy Environ. Sci.*, 7(2013), No. 1, p. 399.
- [6] H.S. Kim, C.R. Lee, J.H. Im, *et al.*, Lead iodide perovskite sensitized all-solid-state submicron thin film mesoscopic solar cell with efficiency exceeding 9%, *Sci. Rep.*, 2(2012), art. No. 591.
- [7] NREL, *Best Research-Cell Efficiencies* [2018-07-16]. <https://www.nrel.gov/pv/assets/images/efficiency-chart-20180716.jpg>
- [8] M. Gratzel, The light and shade of perovskite solar cells, *Nat. Mater.*, 13(2014), No. 9, p. 838.
- [9] S.J. Li, Y. Lin, W.W. Tan, *et al.*, Preparation and performance of dye-sensitized solar cells based on ZnO-modified TiO_2 electrodes, *Int. J. Miner. Metall. Mater.*, 17(2010), No. 1, p. 92.
- [10] M. Saliba, T. Matsui, J.Y. Seo, *et al.*, Cesium-containing triple cation perovskite solar cells: Improved stability, reproducibility and high efficiency, *Energy Environ. Sci.*, 9(2016), No. 6, p. 1989.
- [11] W.S. Yang, B.W. Park, E.H. Jung, *et al.*, Iodide management in formamidinium-lead-halide-based perovskite layers for efficient solar cells, *Science*, 356(2017), No. 6345, p. 1376.
- [12] C.W. Liu, R.X. Zhu, A. Ng, *et al.*, Investigation of high performance TiO_2 nanorod array perovskite solar cells, *J. Mater. Chem. A*, 5(2017), No. 30, p. 15970.
- [13] D.Y. Son, J.H. Im, H.S. Kim, and N.G. Park, 11% efficient perovskite solar cell based on ZnO nanorods: An effective

- charge collection system, *J. Phys. Chem. C*, 118(2014), No. 30, p. 16567.
- [14] J.F. Li, Z.L. Zhang, H.P. Gao, Y. Zhang, and Y.L. Mao, Effect of solvents on the growth of TiO₂ nanorods and their perovskite solar cells, *J. Mater. Chem. A*, 3(2015), No. 38, p. 19476.
- [15] J.Y. Jeng, Y.F. Chiang, M.H. Lee, et al., CH₃NH₃PbI₃ perovskite/fullerene planar-heterojunction hybrid solar cells, *Adv. Mater.*, 25(2013), No. 27, p. 3727.
- [16] H.S. Kim, S.H. Im, and N.G. Park, Organolead halide perovskite: New horizons in solar cell research, *J. Phys. Chem. C*, 118(2014), No. 11, p. 5615.
- [17] F. Aslan, G. Adam, P. Stadler, A. Göktaş, I.H. Mutlu, and N.S. Sariciftci, Sol-gel derived In₂S₃ buffer layers for inverted organic photovoltaic cells, *Sol. Energy*, 108(2014), p. 230.
- [18] G. Yang, H. Tao, P.L. Qin, W.J. Ke, and G.J. Fang, Recent progress in electron transport layers for efficient perovskite solar cells, *J. Mater. Chem. A*, 4(2016), No. 11, p. 3970.
- [19] J.R. Lian, B. Lu, F.F. Niu, P.J. Zeng, and X.W. Zhan, Electron-transport materials in perovskite solar cells, *Small Methods*, 2(2018), No. 10, p. 1800082.
- [20] Y.P. Xia, P.H. Wang, S.W. Shi, et al., Effect of oxygen partial pressure and transparent substrates on the structural and optical properties of ZnO thin films and their performance in energy harvesters, *Int. J. Miner. Metall. Mater.*, 24(2017), No. 6, p. 675.
- [21] P. Gao, M. Grätzel, and M.K. Nazeeruddin, Organohalide lead perovskites for photovoltaic applications, *Energy Environ. Sci.*, 7(2014), No. 8, p. 2448.
- [22] Q. Jiang, X.W. Zhang, and J.B. You, SnO₂: A wonderful electron transport layer for perovskite solar cells, *Small*, 14(2018), No. 31, art. No. 1801154.
- [23] P. Zhang, J. Wu, T. Zhang, et al., Perovskite solar cells with ZnO electron-transporting materials, *Adv. Mater.*, 30(2018), No. 3, art. No. 1703737.
- [24] A. Goktas, F. Aslan, B. Yesilata, and I. Boz, Physical properties of solution processable n-type Fe and Al co-doped ZnO nanostructured thin films: Role of Al doping levels and annealing, *Mater. Sci. Semicon. Process.*, 75(2018), p. 221.
- [25] Z.Q. Zhu and J. Zhou, Rapid growth of ZnO hexagonal tubes by direct microwave heating, *Int. J. Miner. Metall. Mater.*, 17(2010), No. 1, p. 80.
- [26] X.C. Yang, H.X. Wang, B. Cai, Z. Yu, and L.C. Sun, Progress in hole-transporting materials for perovskite solar cells, *J. Energy Chem.*, 27(2018), No. 3, p. 650.
- [27] W.B. Yan, S.Y. Ye, Y.L. Li, et al., Hole-transporting materials in inverted planar perovskite solar cells, *Adv. Energy Mater.*, 6(2016), No. 17, art. No. 1600474.
- [28] M.M. Lee, J. Teuscher, T. Miyasaka, T.N. Murakami, and H.J. Snaith, Efficient hybrid solar cells based on meso-superstructured organometal halide perovskites, *Science*, 338(2012), No. 6107, p. 643.
- [29] M.D. Xiao, F.Z. Huang, W.C. Huang, et al., A fast deposition-crystallization procedure for highly efficient lead iodide perovskite thin-film solar cells, *Angew. Chem.*, 53(2014), No. 37, p. 9898.
- [30] N.J. Jeon, J.H. Noh, Y.C. Kim, W.S. Yang, S. Ryu, and S.I. Seok, Solvent engineering for high-performance inorganic-organic hybrid perovskite solar cells, *Nat. Mater.*, 13(2014), No. 9, p. 897.
- [31] N. Ahn, D.Y. Son, I.H. Jang, S.M. Kang, M. Choi, and N.G. Park, Highly reproducible perovskite solar cells with average efficiency of 18.3% and best Efficiency of 19.7% fabricated via lewis base adduct of lead(II) iodide, *J. Am. Chem. Soc.*, 137(2015), No. 27, p. 8696.
- [32] Q. Chen, H.P. Zhou, Z.R. Hong, et al., Planar heterojunction perovskite solar cells via vapor-assisted solution process, *J. Am. Chem. Soc.*, 136(2014), No. 2, p. 622.
- [33] Z.G. Xiao, C. Bi, Y.C. Shao, et al., Efficient, high yield perovskite photovoltaic devices grown by interdiffusion of solution-processed precursor stacking layers, *Energy Environ. Sci.*, 7(2014), No. 8, p. 2619.
- [34] W.S. Yang, J.H. Noh, N.J. Jeon, et al., High-performance photovoltaic perovskite layers fabricated through intramolecular exchange, *Science*, 348(2015), No. 6240, p. 1234.
- [35] L. Yang, A.T. Barrows, D.G. Lidzey, and T. Wang, Recent progress and challenges of organometal halide perovskite solar cells, *Rep. Prog. Phys.*, 79(2016), No. 2, p. 026501.
- [36] J.H. Noh, S.H. Im, J.H. Heo, T.N. Mandal, and S.I. Seok, Chemical management for colorful, efficient, and stable inorganic-organic hybrid nanostructured solar cells, *Nano Lett.*, 13(2013), No. 4, p. 1764.
- [37] G.D. Niu, X.D. Guo, and L.D. Wang, Review of recent progress in chemical stability of perovskite solar cells, *J. Mater. Chem. A*, 3(2015), No. 17, p. 8970.
- [38] T.A. Berhe, W.N. Su, C.H. Chen, et al., Organometal halide perovskite solar cells: Degradation and stability, *Energy Environ. Sci.*, 9(2016), No. 2, p. 323.
- [39] Q. Jiang, Z.M. Chu, P.Y. Wang, et al., Planar-structure perovskite solar cells with efficiency beyond 21%, *Adv. Mater.*, 29(2017), No. 46, art. No. 1703852.
- [40] D.Y. Son, J.W. Lee, Y.J. Choi, et al., Self-formed grain boundary healing layer for highly efficient CH₃NH₃PbI₃ perovskite solar cells, *Nat. Energy*, 1(2016), No. 7, art. No. 16081.
- [41] D.Q. Bi, C.Y. Yi, J.S. Luo, et al., Polymer-templated nucleation and crystal growth of perovskite films for solar cells with efficiency greater than 21%, *Nat. Energy*, 1(2016), No. 10, art. No. 16142.
- [42] X. Li, D. Bi, C. Yi, et al., A vacuum flash-assisted solution process for high-efficiency large-area perovskite solar cells, *Science*, 353(2016), No. 6294, p. 58.
- [43] N.J. Jeon, J.H. Noh, W.S. Yang, et al., Compositional engineering of perovskite materials for high-performance solar cells, *Nature*, 517(2015), No. 7535, p. 476.
- [44] J.X. Song, W.D. Hu, X.F. Wang, et al., HC(NH₂)₂PbI₃ as a thermally stable absorber for efficient ZnO-based perovskite solar cells, *J. Mater. Chem. A*, 4(2016), No. 21, p. 8435.
- [45] C.H. Chiang, J.W. Lin, and C.G. Wu, One-step fabrication of a mixed-halide perovskite film for a high-efficiency inverted

- solar cell and module, *J. Mater. Chem. A*, 4(2016), No. 35, p. 13525.
- [46] L. Li, N. Liu, Z.Q. Xu, Q. Chen, X.D. Wang, and H.P. Zhou, Precise composition tailoring of mixed-cation hybrid perovskites for efficient solar cells by mixture design methods, *ACS Nano*, 11(2017), No. 9, p. 8804.
- [47] T.Q. Niu, J. Lu, R. Munir, *et al.*, Stable high-performance perovskite solar cells via grain boundary passivation, *Adv. Mater.*, 30(2018), No. 16, art. No. 1706576.
- [48] X.P. Zheng, B. Chen, J. Dai, *et al.*, Defect passivation in hybrid perovskite solar cells using quaternary ammonium halide anions and cations, *Nat. Energy*, 2(2017), No. 7, art. No. 17102.
- [49] Q. Chen, H. Zhou, T.B. Song, *et al.*, Controllable self-induced passivation of hybrid lead iodide perovskites toward high performance solar cells, *Nano Lett.*, 14(2014), No. 7, p. 4158.
- [50] J.Z. Chen, J.Y. Seo, and N.G. Park, Simultaneous improvement of photovoltaic performance and stability by *in situ* formation of 2D perovskite at (FAPbI₃)_{0.88}(CsPbBr₃)_{0.12}/CuSCN interface, *Adv. Energy Mater.*, 8(2018), No. 12, art. No. 1702714.
- [51] H.C. Zai, C. Zhu, H.P. Xie, *et al.*, Congeneric incorporation of CsPbBr₃ nanocrystals in a hybrid perovskite heterojunction for photovoltaic efficiency enhancement, *ACS Energy Lett.*, 3(2017), No. 1, p. 30.
- [52] L. Li, X. Jin, N. Liu, Q. Chen, W.B. Zhang, and H.P. Zhou, Efficient moisture-resistant perovskite solar cell with nanostructure featuring 3D amine motif, *Solar RRL*, 2(2018), No. 9, art. No. 1800069.
- [53] M.A. Green, A. Ho-Baillie, and H.J. Snaith, The emergence of perovskite solar cells, *Nat. Photonics*, 8(2014), No. 7, p. 506.
- [54] Q.X. Fu, X.L. Tang, B. Huang, T. Hu, L.C. Tan, L. Chen, and Y.W. Chen, Recent progress on the long-term stability of perovskite solar cells, *Adv. Sci.*, 5(2018), No. 5, art. No. 1700387.
- [55] W.D. Zhu, C.X. Bao, F.M. Li, *et al.*, A halide exchange engineering for CH₃NH₃PbI_{3-*x*}Br_{*x*} perovskite solar cells with high performance and stability, *Nano Energy*, 19(2016), p. 17.
- [56] Z. Li, M.J. Yang, J.S. Park, S.H. Wei, J.J. Berry, and K. Zhu, Stabilizing perovskite structures by tuning tolerance factor: formation of formamidinium and cesium lead iodide solid-state alloys, *Chem. Mater.*, 28(2016), No. 1, p. 284.
- [57] E. Smecca, Y. Numata, I. Deretzi, *et al.*, Stability of solution-processed MAPbI₃ and FAPbI₃ layers, *Phys. Chem. Chem. Phys.*, 18(2016), No. 19, p. 13413.
- [58] G.E. Eperon, S.D. Stranks, C. Menelaou, M.B. Johnston, L.M. Herz, and H.J. Snaith, Formamidinium lead trihalide: A broadly tunable perovskite for efficient planar heterojunction solar cells, *Energy Environ. Sci.*, 7(2014), No. 3, p. 982.
- [59] Y. Ogomi, A. Morita, S. Tsukamoto, *et al.*, CH₃NH₃Sn_{*x*}Pb_(1-*x*)I₃ perovskite solar cells covering up to 1060 nm, *J. Phys. Chem. Lett.*, 5(2014), No. 6, p. 1004.
- [60] N.K. Noel, S.D. Stranks, A. Abate, *et al.*, Lead-free organo-inorganic tin halide perovskites for photovoltaic applications, *Energy Environ. Sci.*, 7(2014), No. 9, p. 3061.
- [61] F. Hao, C.C. Stoumpos, D.H. Cao, R.P.H. Chang, and M.G. Kanatzidis, Lead-free solid-state organic-inorganic halide perovskite solar cells, *Nat. Photonics*, 8(2014), No. 6, p. 489.
- [62] T.M. Koh, T. Krishnamoorthy, N. Yantara, *et al.*, Formamidinium tin-based perovskite with low *E_g* for photovoltaic applications, *J. Mater. Chem. A*, 3(2015), No. 29, p. 14996.
- [63] W.Q. Liao, D.W. Zhao, Y. Yu, *et al.*, Lead-free inverted planar formamidinium tin triiodide perovskite solar cells achieving power conversion efficiencies up to 6.22%, *Adv. Mater.*, 28(2016), No. 42, p. 9333.
- [64] W.J. Ke, C.C. Stoumpos, M.H. Zhu, *et al.*, Enhanced photovoltaic performance and stability with a new type of hollow 3D perovskite {en}FASnI₃, *Sci. Adv.*, 3(2017), No. 8, art. No. e1701293.
- [65] W.J. Ke, P. Priyanka, S. Vegiraju, *et al.*, Dopant-free tetrakis-triphenylamine hole transporting material for efficient tin-based perovskite solar cells, *J. Am. Chem. Soc.*, 140(2018), No. 1, p. 388.
- [66] Z.R. Zhao, F.D. Gu, Y.L. Li, *et al.*, Mixed-organic-cation tin iodide for lead-free perovskite solar cells with an efficiency of 8.12%, *Adv. Sci.*, 4(2017), No. 11, art. No. 1700204.
- [67] T. Yokoyama, D.H. Cao, C.C. Stoumpos, *et al.*, Overcoming short-circuit in lead-free CH₃NH₃SnI₃ perovskite solar cells via kinetically controlled gas-solid reaction film fabrication process, *J. Phys. Chem. Lett.*, 7(2016), No. 5, p. 776.
- [68] J. Xi, Z.X. Wu, B. Jiao, *et al.*, Multichannel interdiffusion driven FASnI₃ film formation using aqueous hybrid salt/polymer solutions toward flexible lead-free perovskite solar cells, *Adv. Mater.*, 29(2017), No. 23, art. No. 1606964.
- [69] K.P. Marshall, M. Walker, R.I. Walton, and R.A. Hatton, Enhanced stability and efficiency in hole-transport-layer-free CsSnI₃ perovskite photovoltaics, *Nat. Energy*, 1(2016), No. 12, art. No. 16178.
- [70] C.X. Ran, J. Xi, W.Y. Gao, *et al.*, Bilateral interface engineering toward efficient 2D-3D bulk heterojunction tin halide lead-free perovskite solar cells, *ACS Energy Lett.*, 3(2018), No. 3, p. 713.
- [71] I. Chung, B. Lee, J.Q. He, R.P.H. Chang, and M.G. Kanatzidis, All-solid-state dye-sensitized solar cells with high efficiency, *Nature*, 485(2012), No. 7399, p. 486.
- [72] M.H. Kumar, S. Dharani, W.L. Leong, *et al.*, Lead-free halide perovskite solar cells with high photocurrents realized through vacancy modulation, *Adv. Mater.*, 26(2014), No. 41, p. 7122.
- [73] D. Sabba, H.K. Mulmudi, R.R. Prabhakar, *et al.*, Impact of anionic Br⁻ substitution on open circuit voltage in lead free perovskite (CsSnI_{3-*x*}Br_{*x*}) solar cells, *J. Phys. Chem. C*, 119(2015), No. 4, p. 1763.
- [74] S. Gupta, T. Bendikov, G. Hodes, and D. Cahen, CsSnBr₃, a lead-free halide perovskite for long-term solar cell application: Insights on SnF₂ addition, *ACS Energy Lett.*, 1(2016), No. 5, p. 1028.
- [75] D. Moghe, L.L. Wang, C.J. Traverse, *et al.*, All va-

- por-deposited lead-free doped CsSnBr₃ planar solar cells, *Nano Energy*, 28(2016), p. 469.
- [76] N. Wang, Y.Y. Zhou, M.G. Ju, et al., Heterojunction-depleted lead-free perovskite solar cells with coarse-grained B-γ-CsSnI₃ thin films, *Adv. Energy Mater.*, 6(2016), No. 24, art. No. 1601130.
- [77] P. Xu, S.Y. Chen, H.J. Xiang, X.G. Gong, and S.H. Wei, Influence of defects and synthesis conditions on the photovoltaic performance of perovskite semiconductor CsSnI₃, *Chem. Mater.*, 26(2014), No. 20, p. 6068.
- [78] W.Z. Li, J.W. Li, J.L. Li, J.D. Fan, Y.H. Mai, and L.D. Wang, Additive-assisted construction of all-inorganic CsSnI₃ mesoscopic perovskite solar cells with superior thermal stability up to 473 K, *J. Mater. Chem. A*, 4(2016), No. 43, p. 17104.
- [79] L.Z. Zhu, B. Yuh, S. Schoen, et al., Solvent-molecule-mediated manipulation of crystalline grains for efficient planar binary lead and tin triiodide perovskite solar cells, *Nanoscale*, 8(2016), No. 14, p. 7621.
- [80] F. Zuo, S.T. Williams, P.W. Liang, C.C. Chueh, C.Y. Liao, and A.K.Y. Jen, Binary-metal perovskites toward high-performance planar-heterojunction hybrid solar cells, *Adv. Mater.*, 26(2014), No. 37, p. 6454.
- [81] C. Liu, J. Fan, H. Li, C. Zhang, and Y. Mai, Highly efficient perovskite solar cells with substantial reduction of lead content, *Sci. Rep.*, 6(2016), art. No. 35705.
- [82] J.D. Fan, C. Liu, H.L. Li, C.L. Zhang, W.Z. Li, and Y.H. Mai, Molecular Self-assembly fabrication and carrier dynamics of stable and efficient CH₃NH₃Pb_(1-x)Sn_xI₃ perovskite solar cells, *ChemSusChem*, 10(2017), No. 19, p. 3839.
- [83] C. Liu, W.Z. Li, H.L. Li, C.L. Zhang, J.D. Fan, and Y.H. Mai, C₆₀ additive-assisted crystallization in CH₃NH₃Pb_{0.75}Sn_{0.25}I₃ perovskite solar cells with high stability and efficiency, *Nanoscale*, 9(2017), No. 37, p. 13967.
- [84] E. Mosconi, P. Umari, and F. De Angelis, Electronic and optical properties of mixed Sn–Pb organohalide perovskites: A first principles investigation, *J. Mater. Chem. A*, 3(2015), No. 17, p. 9208.
- [85] F. Hao, C.C. Stoumpos, R.P.H. Chang, and M.G. Kanatzidis, Anomalous band gap behavior in mixed Sn and Pb perovskites enables broadening of absorption spectrum in solar cells, *J. Am. Chem. Soc.*, 136(2014), No. 22, p. 8094.
- [86] Y.L. Li, W.H. Sun, W.B. Yan, et al., 50% Sn-based planar perovskite solar cell with power conversion efficiency up to 13.6%, *Adv. Energy Mater.*, 6(2016), No. 24, art. No. 1601353.
- [87] X.B. Xu, C.C. Chueh, Z.B. Yang, et al., Ascorbic acid as an effective antioxidant additive to enhance the efficiency and stability of Pb/Sn-based binary perovskite solar cells, *Nano Energy*, 34(2017), p. 392.
- [88] G. Kapil, T.S. Ripolles, K. Hamada, et al., Highly efficient 17.6% tin–lead mixed perovskite solar cells realized through spike structure, *Nano Lett.*, 18(2018), No. 6, p. 3600.
- [89] S. Lee and D.W. Kang, Highly efficient and stable Sn-rich perovskite solar cells by introducing bromine, *ACS Appl. Mater. Interfaces*, 9(2017), No. 27, p. 22432.
- [90] W.Q. Liao, D.W. Zhao, Y. Yu, et al., Fabrication of efficient low-bandgap perovskite solar cells by combining formamidinium tin iodide with methylammonium lead iodide, *J. Am. Chem. Soc.*, 138(2016), No. 38, p. 12360.
- [91] D.W. Zhao, Y. Yu, C.L. Wang, et al., Low-bandgap mixed tin–lead iodide perovskite absorbers with long carrier lifetimes for all-perovskite tandem solar cells, *Nat. Energy*, 2(2017), No. 4, art. No. 17018.
- [92] N.J. Jeon, H. Na, E.H. Jung, et al., A fluorene-terminated hole-transporting material for highly efficient and stable perovskite solar cells, *Nat. Energy*, 3(2018), No. 8, p. 682.
- [93] D.Y. Luo, W.Q. Yang, Z.P. Wang, et al., Enhanced photovoltage for inverted planar heterojunction perovskite solar cells, *Science*, 360(2018), No. 6396, p. 1442.
- [94] M.M. Tavakoli, S.M. Zakeeruddin, M. Grätzel, and Z.Y. Fan, Large-grain tin-rich perovskite films for efficient solar cells via metal alloying technique, *Adv. Mater.*, 30(2018), No. 11, art. No. 1705998.
- [95] C.M. Tsai, H.P. Wu, S.T. Chang, et al., Role of tin chloride in tin-rich mixed-halide perovskites applied as mesoscopic solar cells with a carbon counter electrode, *ACS Energy Lett.*, 1(2016), No. 6, p. 1086.
- [96] T. Krishnamoorthy, H. Ding, C. Yan, et al., Lead-free germanium iodide perovskite materials for photovoltaic applications, *J. Mater. Chem. A*, 3(2015), No. 47, p. 23829.
- [97] I. Kopacic, B. Friesenbichler, S.F. Hoeffler, et al., Enhanced performance of germanium halide perovskite solar cells through compositional engineering, *ACS Appl. Energy Mater.*, 1(2018), No. 2, p. 343.
- [98] K. Wang, Z.Q. Liang, X.Q. Wang, and X.D. Cui, Lead replacement in CH₃NH₃PbI₃ perovskites, *Adv. Electron. Mater.*, 1(2015), No. 10, art. No. 1500089.
- [99] M. Pazoki, T.J. Jacobsson, A. Hagfeldt, G. Boschloo, and T. Edvinsson, Effect of metal cation replacement on the electronic structure of metalorganic halide perovskites: Replacement of lead with alkaline-earth metals, *Phys. Rev. B*, 93(2016), No. 14, art. No. 144105.
- [100] T.J. Jacobsson, M. Pazoki, A. Hagfeldt, and T. Edvinsson, Goldschmidt's rules and strontium replacement in lead halogen perovskite solar cells: Theory and preliminary experiments on CH₃NH₃SrI₃, *J. Phys. Chem. C*, 119(2015), No. 46, p. 25673.
- [101] M.C. Wu, W.C. Chen, S.H. Chan, and W.F. Su, The effect of strontium and barium doping on perovskite-structured energy materials for photovoltaic applications, *Appl. Surf. Sci.*, 429(2018), p. 9.
- [102] M.C. Wu, T.H. Lin, S.H. Chan, and W.F. Su, Improved efficiency of perovskite photovoltaics based on Ca-doped methylammonium lead halide, *J. Taiwan Inst. Chem. Eng.*, 80(2017), p. 695.
- [103] H.B. Zhang, M.H. Shang, X.Y. Zheng, et al., Ba²⁺ doped CH₃NH₃PbI₃ to tune the energy state and improve the performance of perovskite solar cells, *Electrochim. Acta*, 254(2017), p. 165.

- [104] S.H. Chan, M.C. Wu, K.M. Lee, W.C. Chen, T.H. Lin, and W.F. Su, Enhancing perovskite solar cell performance and stability by doping barium in methylammonium lead halide, *J. Mater. Chem. A*, 5(2017), No. 34, p. 18044.
- [105] X.X. Shai, L.J. Zuo, P.Y. Sun, *et al.*, Efficient planar perovskite solar cells using halide Sr-substituted Pb perovskite, *Nano Energy*, 36(2017), p. 213.
- [106] C.F.J. Lau, M. Zhang, X.F. Deng, *et al.*, Strontium-doped low-temperature-processed CsPbI₂Br perovskite solar cells, *ACS Energy Lett.*, 2(2017), No. 10, p. 2319.
- [107] D. Perez-Del-Rey, D. Forgács, E.M. Hutter, *et al.*, Strontium insertion in methylammonium lead iodide: Long charge carrier lifetime and high fill-factor solar cells, *Adv. Mater.*, 28(2016), No. 44, p. 9839.
- [108] H. Zhang, H. Wang, S.T. Williams, *et al.*, SrCl₂ derived perovskite facilitating a high efficiency of 16% in hole-conductor-free fully printable mesoscopic perovskite solar cells, *Adv. Mater.*, 29(2017), No. 15, art. No. 1606608.
- [109] P.P. Boix, S. Agarwala, T.M. Koh, N. Mathews, and S.G. Mhaisalkar, Perovskite solar cells: Beyond methylammonium lead iodide, *J. Phys. Chem. Lett.*, 6(2015), No. 5, p. 898.
- [110] Z.H. Nie, J. Yin, H.W. Zhou, *et al.*, Layered and Pb-free organic-inorganic perovskite materials for ultraviolet photoresponse: (010)-oriented (CH₃NH₃)₂MnCl₄ thin film, *ACS Appl. Mater. Interfaces*, 8(2016), No. 41, p. 28187.
- [111] X.P. Cui, K.J. Jiang, J.H. Huang, *et al.*, Cupric bromide hybrid perovskite heterojunction solar cells, *Synth. Met.*, 209(2015), p. 247.
- [112] D. Cortecchia, H.A. Dewi, J. Yin, *et al.*, Lead-free MA₂CuCl₃Br_{4-x} hybrid perovskites, *Inorg. Chem.*, 55(2016), No. 3, p. 1044.
- [113] X.L. Li, B.C. Li, J.H. Chang, *et al.*, (C₆H₅CH₂NH₃)₂CuBr₄: A lead-free, highly stable two-dimensional perovskite for solar cell applications, *ACS Appl. Energy Mater.*, 1(2018), No. 6, p. 2709.
- [114] X.X. Liu, T.J. Huang, L.Y. Zhang, *et al.*, Highly stable, new, organic-inorganic perovskite (CH₃NH₃)₂PdBr₄: Synthesis, structure, and physical properties, *Chemistry*, 24(2018), No. 19, p. 4991.
- [115] L.A. Frolova, D.V. Anokhin, K.L. Gerasimov, N.N. Dremova, and P.A. Troshin, Exploring the effects of the Pb²⁺ substitution in MAPbI₃ on the photovoltaic performance of the hybrid perovskite solar cells, *J. Phys. Chem. Lett.*, 7(2016), No. 21, p. 4353.
- [116] M. Jahandar, J.H. Heo, C.E. Song, *et al.*, Highly efficient metal halide substituted CH₃NH₃I(PbI₂)_{1-x}(CuBr₂)_x planar perovskite solar cells, *Nano Energy*, 27(2016), p. 330.
- [117] J.J. Jin, H. Li, C. Chen, *et al.*, Enhanced performance of perovskite solar cells with zinc chloride additives, *ACS Appl. Mater. Interfaces*, 9(2017), No. 49, p. 42875.
- [118] M.T. Klug, A. Osherov, A.A. Haghighirad, *et al.*, Tailoring metal halide perovskites through metal substitution: Influence on photovoltaic and material properties, *Energy Environ. Sci.*, 10(2017), No. 1, p. 236.
- [119] M. Li, Z.K. Wang, M.P. Zhuo, *et al.*, Pb–Sn–Cu ternary organometallic halide perovskite solar cells, *Adv. Mater.*, 30(2018), No. 20, p. art. No. 1800258.
- [120] S. Niki, M. Contreras, I. Repins, *et al.*, CIGS absorbers and processes, *Prog. Photovolt: Res. Appl.*, 18(2010), No. 6, p. 453.
- [121] S.Y. Chen, A. Walsh, X.G. Gong, and S.H. Wei, Classification of lattice defects in the kesterite Cu₂ZnSnS₄ and Cu₂ZnSnSe₄ earth-abundant solar cell absorbers, *Adv. Mater.*, 25(2013), No. 11, p. 1522.
- [122] H.P. Zhou, W.C. Hsu, H.S. Duan, *et al.*, CZTS nanocrystals: A promising approach for next generation thin film photovoltaics, *Energy Environ. Sci.*, 6(2013), No. 10, p. 2822.
- [123] J. Zhang, M.H. Shang, P. Wang, *et al.*, n-Type doping and energy states tuning in CH₃NH₃Pb_{1-x}Sb_{2x/3}I₃ perovskite solar cells, *ACS Energy Lett.*, 1(2016), No. 3, p. 535.
- [124] T. Oku, Y. Ohishi, and A. Suzuki, Effects of antimony addition to perovskite-type CH₃NH₃PbI₃ photovoltaic devices, *Chem. Lett.*, 45(2016), No. 2, p. 134.
- [125] S. Chatterjee, U. Dasgupta, and A.J. Pal, Sequentially deposited antimony-doped CH₃NH₃PbI₃ films in inverted planar heterojunction solar cells with a high open-circuit voltage, *J. Phys. Chem. C*, 121(2017), No. 37, p. 20177.
- [126] G.E. Eperon, G.M. Paterno, R.J. Sutton, *et al.*, Inorganic caesium lead iodide perovskite solar cells, *J. Mater. Chem. A*, 3(2015), No. 39, p. 19688.
- [127] Y.Q. Hu, F. Bai, X.B. Liu, *et al.*, Bismuth incorporation stabilized α -CsPbI₃ for fully inorganic perovskite solar cells, *ACS Energy Lett.*, 2(2017), No. 10, p. 2219.
- [128] Z.K. Wang, M. Li, Y.G. Yang, *et al.*, High efficiency Pb–In binary metal perovskite solar cells, *Adv. Mater.*, 28(2016), No. 31, p. 6695.
- [129] A. Singh, K.M. Boopathi, A. Mohapatra, Y.F. Chen, G. Li, and C.W. Chu, Photovoltaic performance of vapor-assisted solution-processed layer polymorph of Cs₃Sb₂I₉, *ACS Appl. Mater. Interfaces*, 10(2018), No. 3, p. 2566.
- [130] P.C. Harikesh, H.K. Mulmudi, B. Ghosh, *et al.*, Rb as an alternative cation for templating inorganic lead-free perovskites for solution processed photovoltaics, *Chem. Mater.*, 28(2016), No. 20, p. 7496.
- [131] J.C. Hebig, I. Kühn, J. Flohre, and T. Kirchartz, Optoelectronic properties of (CH₃NH₃)₃Sb₂I₉ thin films for photovoltaic applications, *ACS Energy Lett.*, 1(2016), No. 1, p. 309.
- [132] M. Abulikemu, S. Ould-Chikh, X.H. Miao, *et al.*, Optoelectronic and photovoltaic properties of the air-stable organohalide semiconductor (CH₃NH₃)₃Bi₂I₉, *J. Mater. Chem. A*, 4(2016), No. 32, p. 12504.
- [133] M.B. Johansson, H.M. Zhu, and E.M.J. Johansson, Extended photo-conversion spectrum in low-toxic bismuth halide perovskite solar cells, *J. Phys. Chem. Lett.*, 7(2016), No. 17, p. 3467.
- [134] C. McDonald, C.S. Ni, V. Švrček, *et al.*, Zero-dimensional methylammonium iodo bismuthate solar cells and synergistic interactions with silicon nanocrystals, *Nanoscale*, 9(2017), No. 47, p. 18759.
- [135] T. Singh, A. Kulkarni, M. Ikegami, and T. Miyasaka, Effect

- of electron transporting layer on bismuth-based lead-free perovskite $(\text{CH}_3\text{NH}_3)_3\text{Bi}_2\text{I}_9$ for photovoltaic applications, *ACS Appl. Mater. Interfaces*, 8(2016), No. 23, p. 14542.
- [136] Y. Kim, Z.Y. Yang, A. Jain, *et al.*, Pure cubic-phase hybrid iodobismuthates AgBi_2I_7 for thin-film photovoltaics, *Angew. Chem. Int. Ed.*, 128(2016), No. 33, p. 9586.
- [137] B.W. Park, B. Philippe, X.L. Zhang, H. Rensmo, G. Boschloo, and E.M.J. Johansson, Bismuth based hybrid perovskites $\text{A}_3\text{Bi}_2\text{I}_9$ (A: methylammonium or cesium) for solar cell application, *Adv. Mater.*, 27(2016), No. 43, p. 6806.
- [138] C.X. Ran, Z.X. Wu, J. Xi, *et al.*, Construction of compact methylammonium bismuth iodide film promoting lead-free inverted planar heterojunction organohalide solar cells with open-circuit voltage over 0.8 V, *J. Phys. Chem. Lett.*, 8(2017), No. 2, p. 394.
- [139] S.S. Shin, J.P.C. Baena, R.C. Kurchin, *et al.*, Solvent-engineering method to deposit compact bismuth-based thin films: Mechanism and application to photovoltaics, *Chem. Mater.*, 30(2018), No. 2, p. 336.
- [140] A.H. Slavney, T. Hu, A.M. Lindenberg, and H.I. Karunadasa, A bismuth-halide double perovskite with long carrier recombination lifetime for photovoltaic applications, *J. Am. Chem. Soc.*, 138(2016), No. 7, p. 2138.
- [141] E.T. McClure, M.R. Ball, W. Windl, and P.M. Woodward, $\text{Cs}_2\text{AgBiX}_6$ (X = Br, Cl): New visible light absorbing, lead-free halide perovskite semiconductors, *Chem. Mater.*, 28(2016), No. 5, p. 1348.
- [142] G. Volonakis, M.R. Filip, A.A. Haghighirad, *et al.*, Lead-free halide double perovskites via heterovalent substitution of noble metals, *J. Phys. Chem. Lett.*, 7(2016), No. 7, p. 1254.
- [143] F.X. Wei, Z.Y. Deng, S.J. Sun, *et al.*, The synthesis, structure and electronic properties of a lead-free hybrid inorganic-organic double perovskite $(\text{MA})_2\text{KBiCl}_6$ (MA = methylammonium), *Mater. Horiz.*, 3(2016), No. 4, p. 328.
- [144] F.X. Wei, Z.Y. Deng, S.J. Sun, *et al.*, Synthesis and properties of a lead-free hybrid double perovskite: $(\text{CH}_3\text{NH}_3)_2\text{AgBiBr}_6$, *Chem. Mater.*, 29(2017), No. 3, p. 1089.
- [145] E. Greul, M.L. Petrus, A. Binek, P. Docampo, and T. Bein, Highly stable, phase pure $\text{Cs}_2\text{AgBiBr}_6$ double perovskite thin films for optoelectronic applications, *J. Mater. Chem. A*, 5(2017), No. 37, p. 19972.
- [146] W.H. Ning, F. Wang, B. Wu, *et al.*, Long electron-hole diffusion length in high-quality lead-free double perovskite films, *Adv. Mater.*, 30(2018), No. 20, art. No. 1706246.
- [147] C.C. Wu, Q.H. Zhang, Y. Liu, *et al.*, The dawn of lead-free perovskite solar cell: Highly stable double perovskite $\text{Cs}_2\text{AgBiBr}_6$ film, *Adv. Sci.*, 5(2018), No. 3, art. No. 1700759.
- [148] W.Y. Gao, C.X. Ran, J. Xi, *et al.*, High-quality $\text{Cs}_2\text{AgBiBr}_6$ double perovskite film for lead-free inverted planar heterojunction solar cells with 2.2% efficiency, *ChemPhysChem*, 19(2018), No. 14, p. 1696.
- [149] G. Volonakis, A.A. Haghighirad, R.L. Milot, *et al.*, $\text{Cs}_2\text{InAgCl}_6$: A new lead-free halide double perovskite with direct band gap, *J. Phys. Chem. Lett.*, 8(2017), No. 4, p. 772.